Detection of decarburising depth in Hadfield steels using a multi-magnetic NDE method

Saeed Kahrobaee[1], Iman Ahadi Akhlaghi[2] and Claire Davis[3]

[1] Department of Mechanical and Materials Engineering, Sadjad University, Mashhad, Iran

[2] Department of Electrical and Biomedical Engineering, Sadjad University, Mashhad, Iran

[3] Advanced Steel Research Centre, Warwick Manufacturing Group, University of Warwick, Coventry, UK

Corresponding author: Tel.: +98 5136029000; fax: +98 5136029110, E-mail addresses: kahrobaee@sadjad.ac.ir, saeed.kahrobaee@gmail.com (Saeed Kahrobaee)

1- Assistant Professor, Department of Mechanical and Materials Engineering, Sadjad University, Mashhad, Iran, kahrobaee@sadjad.ac.ir

2- Associate Professor, Department of Electrical and Biomedical Engineering, Sadjad University, Mashhad, Iran, i_a_akhlaghi@sadjad.ac.ir

3- Professor, Advanced Steel Research Centre, Warwick Manufacturing Group, University of Warwick, Coventry, UK, claire.davis@warwick.ac.uk

Detection of decarburising depth in Hadfield steels using a multi-magnetic NDE method

Abstract

This paper reports the capability of different widely used electromagnetic nondestructive evaluation (NDE) methods to characterise the decarburising phenomena in Hadfield steels. As a result of austenitisation in an uncontrolled atmosphere, a thin layer of martensite phase forms at the Hadfield steel surface after quenching, which is attributed to decarburising. In this work, to produce various decarburising depths, four Hadfield steel samples were austenitised at 1050 °C for 1, 2, 3 and, 4 hours in an air furnace and then quenched in water. The depth of the decarburised layers was characterized using hardness profile measurements, optical and scanning electron microscopy as well as X-ray diffraction analysis. The results confirmed the occurrence of decarburising and presence of a surface martensite layer of 35 to 110 μm depending on austenitisation time. The microstructural change at the surface affects the magnetic properties of the sample and enables electromagnetic NDE methods to detect the transformed layers, quantitatively. In the nondestructive characterisation step, the relationships between the austenitising time and the outputs from magnetic flux leakage (MFL), initial magnetisation curve (BH) and eddy current (EC) methods are reported. Comparing the results obtained from the three magnetic NDE methods, it can be concluded that MFL and EC (phase angle output) have the potential to quantify the surface microstructural changes occurring as a result of the decarburising process in Hadfield steels.

Keywords: Hadfield steel, Decarburising depth, Magnetic flux leakage, Initial magnetisation curve and Eddy current

1. Introduction

In the literature, it is reported that controlled heat treatment cycles including austenitising, quenching and tempering treatments are necessary to optimise the microstructural characteristics of modified Hadfield austenitic manganese steels [1]. Hadfield steels are usually austenitised above 1050 °C to dissolve carbides; then, quenching in water is done to obtain a uniform austenitic structure [2, 3]. However, in the absence of a vacuum furnace or an inert atmosphere, a high austenitising temperature often produces surface decarburisation and a reduction in local manganese content, leading to an increase in the martensite start (Ms) temperature. Thus, transformation of austenite to α-martensite at the surface layer can occur after quenching. In addition, a number of papers have reported that strain-induced transformation to martensite can also occur due to decarburisation or local segregation of manganese and therefore formation of a meta-stable austenite composition [2, 4, 5, 6].

Gruzin et al. [6] have presented details of the austenite to martensite transformation in austenitic manganese steel. Their work can be summarised as follows: As a result of decarburisation of the γ solid solution at high solutionising temperature, manganese diffuses into the carbides. In this situation, all the carbon is concentrated in the carbide phase with negligible carbon in solid solution. Thus, γ (1.25 wt% C) is converted to γ (0.05 - 0.15 wt%C) and eutectoid (α + $(Fe, Mn)_3C$) mixture. Finally, ε- and α-martensite phases, are formed from decarburised austenite by the reaction of γ (0.05 - 0.15 wt%C) → ε + α (martensite). Thus, Hadfield steel should not be subjected to a heat-treating process in an uncontrolled or weakly oxidising atmosphere unless the decarburised layer is removed before use.

According to the International Standard ISO 3887, the conventional methods to detect and quantify the occurrence of decarburisation are microstructural observation using metallography and plotting the hardness profile by micro-hardness measurements. In the last

decade, nondestructive evaluation (NDE) technologies have enabled inspection systems to characterise the microstructural changes at the surface of heat-treated steel parts. For example, detection of a carburised layer [7, 8], induction hardened depth [9, 10, 11] and nitrided layer [12] are some applications of NDE methods to determine the microstructural changes at the surface. Particularly, detection of the various microstructures that can form in decarburised layers has been studied. For instance, a high ferrite/low pearlite layer over a low ferrite/high pearlite layer in AISI 1045 has been characterised using the evaluation of relationship between EC impedance point and decarburizing depth [13]. In [14], The same microstructural change has been detected in AISI 1055 steel using MBN technique, where the position of the MBN peaks was used to estimate the thickness of the decarburised layer. In [15], a multi-frequency electromagnetic sensor was used to nondestructively evaluate a full ferrite layer on a full pearlitic microstructure in AISI 1080 steel, relating the inductance value to decarburised layer depth. The MBN coercivity was proposed in [16] as a new electromagnetic parameter to detect a full ferrite layer on the ferrite/pearlite microstructure in spring steel after acid pickling and sand blasting treatments. A ferrite layer on a martensite core in SAE 92V45 steel has also been determined using harmonic decomposition of EC signals in [17]. In [18], the capability of the MBN technique to detect a ferrite/pearlite layer on a tempered martensite has been reported for Ovako 677 steel. Finally, a decarburised ferrite layer on the normal rail steel microstructure of pearlite has been assessed quantitatively using a multi-frequency electromagnetic sensor in [19]. However, the formation of martensite phase as a decarburised layer on the austenitic matrix of Hadfield steel has not yet been evaluated using nondestructive techniques.

In our recent investigations on Hadfield steels, the ability of the EC method for characterising carbide/pearlite precipitation on austenitic grain boundaries as a result of inappropriate applied heat treatment [20] and the amount of work-hardening of the Hadfield steel subjected to hammering treatment [21] have been reported. In the present paper, the

capabilities of three magnetic NDE methods, including magnetic flux leakage (MFL), initial magnetisation (BH) curves and EC for determining the decarburising depth of Hadfield steels have been studied. These methods are widely used for microstructural characterisation and have been considered as they are based on similar electromagnetic phenomena.

2. Experimental Procedure

To create different decarburising depths in Hadfield steel, five samples with dimensions of 100 mm × 20 mm × 4mm were prepared. Four samples were austenitised at 1050 °C in an air furnace for 1, 2, 3 and 4 hours followed by water quenching and one was left as-received without any decarburised layer (austenitising time of 0 in the air furnace). For the as-received sample, to ensure that a decarburised layer does not form on the surface, but the same bulk microstructure was achieved it was separately austenitised in an argon atmosphere furnace at 1050 °C followed by water quenching at ambient temperature. Microstructural changes in the bulk and at the surface of the decarburised samples were studied using optical (Motic BA310MET) and scanning electron microscopes (SEM VP 1450) as well as X-ray diffraction diffractometer (X'Pert Philips). Besides plotting the hardness profiles of the samples using the Vickers indenter on a Bohler micro-hardness tester (25 g load for 10 seconds), the decarburised depths were also measured from the optical and SEM images.

To non-destructively characterise the microstructure of a given steel sample, based on the results of the MFL, BH and EC methods, the experimental setups, shown in the schematic block diagram of Fig. 1, were used. The excitation part in the MFL and MHL (used to generate the BH curves) subsystems is similar and so, the tested location and the magnetisation state of material are identical for these methods.

In order to magnetise the steel samples in the MFL and MHL (BH) subsystems, two 1500-turn coils connected in-series were used, each wound on one arm of a U-shape core. A

triangular signal was made using a LabVIEW program. The signal was then amplified using a current amplifier with a specified frequency and amplitude to excite the magnetising coils. The two-stage bi-polar amplifier used in this research has been originally designed in our laboratory and is completely linear. Our measurements confirmed that the excitation current of the magnetising coils was directly proportional to the output waveform of the Advantech PCI-1720U-AE D/A conversion card installed on a desktop computer with the Windows 10 operating system. The amplifier could provide 1A current, which was sufficient to magnetically saturate our steel samples. According to the measurements, discussed in the following sections, Bmax values for all the samples are less than 0.7 T.

A Hall-effect sensor (HW-108C) at 0.5 mm above the sample was used to gauge the surface field for the MFL subsystem. Other than magnetising coils, two in-series coils with 1000 turns of copper wire (0.1 mm diameter) on the same U-shape core, were used to measure the magnetic field induced into the steel samples. Hall-effect sensor and sensing coils outputs were sampled with a sampling rate of 500 samples/s and the precision of 12 bits using an Advantech PCI-1714UL-BE A/D conversion card installed on the same computer. The measured voltage (from the sensing coils) induced into the steel samples (emf) was then scaled and time-integrated using a MATLAB program in order to provide the B-field.

In addition to the B-field, the magnetic field strength (H-field) was also required to plot the B-H curve. The magnetising waveform, available from the LabVIEW program, could be considered as the H-field after some scaling, since the magnetic field strength was perfectly proportional to the exciting current, as mentioned above. It should also be noted that although all magnetic parameters (including H-field) were accurately measured using our measurement system, the exact values were not important as their relative values are enough for characterising the decarburisation behaviour. Using both B-field and H-field, it is possible to plot the B-H curve and compute the Bmax.

One coaxial excitation coil and one pickup coil, each with a length of 30 mm, were applied in the EC subsystem in order to respectively magnetise the steel samples and to measure the induced voltage in them. The excitation and pickup coils had respectively 200 and 400 turns of fine copper wire. A sinusoidal signal generated using a laboratory function generator with the frequency range of 1-100 kHz was fed to the excitation coil after an appropriate current amplification and when the sample was demagnetised. Since any residual field can affect the results significantly, demagnetisation between measurements is mandatory. This process is done by applying a sinusoidal voltage with a reducing amplitude to the excitation coils. The measured induced voltage, which was the output of the pickup coil, was then given to another analog port of the Advantech PCI-1714UL-BE A/D conversion card. A MATLAB program finally computed the root mean square (RMS) of the induced voltage of the pickup coil, normalised impedance (Z/Z0) and the phase angle (ϕ) of the excitation coil in the presence of the steel sample under test.

3. Results and Discussion

The recommended ISO 3887 method for measuring the decarburised depth is determining the micro-hardness profile on a cross section of the steel sample after polishing. Therefore, in the present work, the relationship between the microstructure in the decarburised zone and micro-hardness value has been evaluated. According to ISO 3887, the depth of decarburisation is considered as the distance between the surface of the sample and the point at which the hardness is at the level where the performance would be unaffected by a reduction in hardness, which is equivalent to the bulk hardness for the Hadfield steels. Fig. 2 presents the hardness profiles of the four steel samples, subjected to different austenitising times. Contrary to what is expected in the decarburisation process for conventional carbon steels where hardness decreases in the decarburised region, in all the Hadfield steel samples, an increase in

the hardness is observed towards the surface from the material core and in the core the hardness has a constant value. The thickness of decarburised layers has been determined by considering a depth where hardness becomes constant and equal to the bulk hardness. Fig. 2 indicates the heat-treating process in the absence of an inert atmosphere increases the hardness of the surface by at least 300 HV compared to the bulk (for the sample austenitised for 1 hour), which is attributed to the surface microstructural changes as a result of the decarburisation process. An increase in the austenitising time increases the hardness in the surface region (from 590 to 900 HV) and increases the hardening depth (from 35 to 110 μm) for the samples. This is expected to be due to the amount and depth of the hard martensite phase formed at the surface. It should be noted that a gradual decreasing trend in micro-hardness values indicates the existence of a martensite-austenite mixture in the decarburised layer where the amount of austenite phase increases with depth.

Fig. 3 shows optical images of the cross sectioned Hadfield steel sample showing the surface subjected to different durations of austenitising treatment. A single austenite phase, with large grain size, is seen for the as-received sample at the surface. However, it is observed that the surface microstructures of the heat-treated samples (in the air furnace) are different. For all the heat treated samples, close to the surface a thin layer with a clear boundary to the austenite grains is seen. For the samples austenitised for longer durations, significant increases in the decarburised layer thickness are observed, which in turn confirms the relationships of austenitising time and decarburising phenomena. As it can be seen, the present observations are in good agreement with the reported results in micro-hardness investigations.

To support the micro-hardness and optical microscopic observations, SEM examinations were also carried out to explore the phase characteristics formed in the surface layer. The SEM images, showing the microstructures of the core and decarburised layer of the section austenitised for 4 hours, are shown in Fig. 4. A relatively clear boundary between the

martensite and austenite phases at about 110 μm (measured by an image processing software) below the surface is seen in Fig. 4a. Single austenite phase is observed in the core microstructure of the decarburised sample (Fig. 4b). It can also be seen that martensite phase has been formed at the surface of the sample (Fig. 4c). At higher magnifications (Figs. 4d and 4e) the needle structure of martensite is observed.

To evaluate the phases formed in the decarburised layer, XRD analysis was performed. The results of XRD are presented in Fig. 5. It can be clearly seen, in the as-received sample, five peaks corresponding to 2θ angles of 43.47°, 50.67°, 74.67°, 90.67°, and 95.94° appear respectively for the (111), (200), (220), (311), and (222) planes of the austenitic phase. However, the XRD graphs from the surface of the decarburised samples confirm the formation of martensite phase due to the appearance of (110), (200), (211), and (220) planes of martensite at 2θ = 44.67°, 65.02°, 82.33°, and 98.94°. For the sample with the austenitising time of 1 hour, the peaks of austenite phase were not removed completely, while the martensite ones are clearly present. This means that at the surface of the sample (with a penetration depth of less than about 20 microns, measured by XRD), the microstructure contains austenite (in a low content) and martensite. With an increasing depth of decarburised layer, the intensity of the martensite peaks increased and the austenite peaks were completely eliminated. Indeed, the loss of manganese and carbon from solid solution at the surface during heat treatment in an air atmosphere [4, 6] results in a thin layer of martensite at the surface of the Hadfield steel, if an inert atmosphere is not available.

In Fig. 6a, the MFL induced voltage has been plotted with respect to the decarburising depths resulting from different austenitising times of 0, 1, 2, 3 and 4 hours. As it is clearly observed, all the induced voltage plots perfectly follow the triangular waveform used to excite the samples. As expected, the amplitude of the induced voltage has a reverse relationship with the depth of decarburisation. This can also be seen in Fig. 6b, where the MFL Vp-p is plotted

with respect to the decarburising depth. This is because at the longer durations of the austenitisation treatment, more decarburising occurs and there is more paramagnetic austenite to ferromagnetic martensite transformation in the surface region. Therefore, in the presence of a martensite layer, the magnetic flux lines are concentrated at the surface and less leakage occurs from the surface. This also causes the Hall sensor to sense less flux near the surface. Accordingly, growth in the decarburised martensite layer at the surface reduces the MFL output dramatically.

In Fig. 7a, the magnetic flux density has been plotted with respect to the magnetic field strength for different decarburising depths of 0, 35, 55, 65 and 110 µm. As it can be seen, due to the paramagnetic nature of Hadfield steel, the hysteresis effect is not observed. There is no clear distinction between the B-H curves for different samples in this figure. In Fig. 7b, the maximum measured value of B (Bmax) for the applied H is plotted with respect to the decarburising depth, where it can be seen that there is a relationship between Bmax and the decarburising depth. However, this relationship is not as clear as seen in Fig. 6b, especially for the decarburising depths of 35, 55 and 65 µm. The low performance of the B-H results is attributed to the fact that Bmax measured in the B-H method is more affected by the volumetric properties of the austenite phase than the thin layer of martensite at the surface, since for the excitation frequency of 0.1 Hz the penetrating depth is much larger than thickness of the decarburized layer.

In the graphs shown in Fig. 8 the RMS voltage, normalised impedance and phase angle of the eddy current induced into the samples are plotted with respect to the decarburising depth. As it is seen, all the parameters have a clear direct relationship with the decarburising depth. Therefore, they also can be used to estimate the amount of decarburising and associated austenite to martensite transformation at the surface of the samples. The improved performance of the EC method to identify the surface microstructures in comparison with the BH method is

attributed to the fact that the EC method works at higher frequencies in which the skin effect is dominant. Indeed, according to the equation for the penetration depth [22], at the operating frequency of 40 kHz, the skin depth for all our Hadfield steel samples is slightly more than 120µm, if a decarburised martensite layer is present (relative permeability and electrical conductivity values in skin depth equation were considered for surface martensitic microstructure; μr=75 and σ=0.41×10^7 Ω^{-1} m^{-1}).

Indeed, the penetration depth formula gives just an approximate value as, for example, the specific sensor geometry is not considered, and the depth is where the magnetic field reduces to exp (-1) ≈ 0.37 of its initial value, therefore the material below this depth also affects the signal albeit with less effect. Therefore, when implementing the eddy current method, the exact frequency that gives the best resolution for the surface layers being measured must be chosen experimentally. In our case, we have swept the frequency range from 15 to 50 kHz to find the frequency in which the eddy current method has the best performance. The frequency of 40 kHz was chosen according to this experimental study.

The calculated skin depth for a fully martensitic layer with 40 kHz measurement frequency is almost equal to the maximum decarburised depth measured for these samples, and hence the contribution of the decarburised layer to the inductance is much higher than that of the austenitic phase and the sensitivity of the method is maximum near the operating frequency of 40 kHz. However, the eddy current method is quite a robust technique and the experimental trials showed that any frequency between 38 to 42 kHz could be considered as a suitable penetration frequency.

According to the plots in Figs. 6b, 7b and 8, almost all the magnetic parameters from the three MFL, BH and EC subsystems have a clear relationship with the decarburisation depth. Indeed, according to Fig. 7b, Bmax is the only magnetic parameter that does not have a one-to-one relationship with the decarburisation depth; i.e., if Bmax is used to estimate the

decarburisation depth, an ambiguity is inevitable when it is between 0.656 and 0.658 (T). In Fig. 9, the parameters normalised to the as-received sample have been plotted and the relevant ease by which the signals distinguish between the samples can be visually shown. Normalisation helps compare the outputs of the different methods and select the best one (the one that distinguishes the samples from each other more clearly). Despite the clear relationship between each of the magnetic parameters and the decarburisation depth, the plot in Fig. 9 shows that amongst all, the EC phase angle and MFL output show more obvious trends than the other parameters. Hence, it seems that these parameters are best suited to nondestructively estimate the decarburising depth. Besides, as can be clearly seen, since the MFL points have a more linear relationship with decarburising depth, the regression line is fitted with a higher R-square measure, in comparison with the EC phase angle.

4. Conclusions

In the present paper the ability of three widely used electromagnetic NDE methods (MFL, BH and EC) to characterise the decarburisation depth in Hadfield steels is studied. The main results are as follows:

1. As a result of the heat-treating process applied to the Hadfield steels in an air furnace, decarburisation phenomena occurred, which results in the formation of a thin martensite layer at the surface of the steel sample. Formation of this ferromagnetic phase on the paramagnetic Hadfield steels enables the magnetic nondestructive inspection systems to determine the surface microstructural changes. The results of XRD and SEM evaluations confirmed the occurrence of the austenite to martensite transformation in the decarburised layers. An increase in austenitising time from 1 to 4 hours, increases the surface hardness (from 590 to 900 HV) and decarburising depth (from 35 to 110 μm).

2. In nondestructive evaluation of the decarburising depth, it was found that: (i) MFL is the preferred method to detect the occurrence of decarburisation and to determine the decarburising depth, quantitatively. The results from the MFL method to determine the decarburising depth represent a similar accuracy to the micro-hardness test (The correlation coefficient of linear relationship between the MFL outputs and the values of decarburizing depths obtained from micro-hardness method is about 0.98). (ii) BH measurement system is not sensitive enough to distinguish the samples with different decarburised layers from each other. This is because the Bmax is more influenced by the magnetic properties of the bulk which is paramagnetic in Hadfield steels; (iii) the phase angle from the EC measurement system shows a semi-linear variation (R^2=0.89) for the different decarburising depths. Therefore, although the MFL method is advised, the phase angle of EC also can be used as a good technique to characterise the decarburising depth.

References

1. Smith R, DeMonte A, Mackay W: Development of high-manganese steels for heavy duty cast-to-shape applications. Journal of Materials Processing Technology; 153-154:589-595.
2. Srivastava AK, Das K. Microstructural characterization of Hadfield austenitic manganese steel. Journal of Materials Science. 2008;43(16):5654-5658.
3. Hosseini S, Limooei M, Zade MH, et al. Optimization of Heat Treatment Due to Austenising Temperature, Time and Quenching Solution in Hadfield Steels. World Academy of Science, Engineering and Technology. 2013;7:1940-1943.
4. Sant S, Smith R. A study in the work-hardening behaviour of austenitic manganese steels. Journal of Materials Science. 1987;22(5):1808-1814.
5. Sil'man G, Pristuplyuk N, Frol'tsov M. Effect of vanadium on the structure and properties of high-manganese steels. Metal Science and Heat Treatment. 1980;22(2):124-127.

6. Gruzin P, Grigorkin V, Moskaleva L. Transformations in austenitic manganese steel. Metal Science and Heat Treatment. 1969;11(1):5-8.
7. Amiri MS, Kashefi M. Application of eddy current nondestructive method for determination of surface carbon content in carburized steels. NDT & E International. 2009;42(7):618-621.
8. Zhang C, Bowler N, Lo C. Magnetic characterization of surface-hardened steel. Journal of Magnetism and Magnetic Materials. 2009;321(23):3878-3887.
9. Kahrobaee S, Kashefi M. Hardness profile plotting using multi-frequency multi-output electromagnetic sensor. NDT & E International. 2011;44(4):335-338.
10. Kashefi M, Kahrobaee S. Dual-frequency approach to assess surface hardened layer using NDE technology. Journal of materials engineering and performance. 2013;22(4):1108-1112.
11. Kahrobaee S, Hejazi T-H, Akhlaghi IA. Electromagnetic methods to improve the nondestructive characterization of induction hardened steels: A statistical modeling approach. Surface and Coatings Technology. 2019;380:125074.
12. Stupakov A, Farda R, Neslušan M, et al. Evaluation of a Nitrided Case Depth by the Magnetic Barkhausen Noise. Journal of Nondestructive Evaluation. 2017;36(4):73.
13. Kahrobaee S, Kashefi M, Alam AS. Magnetic NDT Technology for characterization of decarburizing depth. Surface and Coatings Technology. 2011;205(16):4083-4088.
14. Falahat S, Ghanei S, Kashefi M. Nondestructive examination of decarburised layer of steels using eddy current and magnetic Barkhausen noise testing techniques. Nondestructive Testing and Evaluation. 2018;33(2):154-164.
15. Hao X, Yin W, Strangwood M, et al. Off-line measurement of decarburization of steels using a multifrequency electromagnetic sensor. Scripta Materialia. 2008;58(11):1033-1036.
16. Stupakov O, Perevertov O, Tomáš I, et al. Evaluation of surface decarburization depth by magnetic Barkhausen noise technique. Journal of magnetism and magnetic materials. 2011;323(12):1692-1697.
17. Mercier D, Lesage J, Decoopman X, et al. Eddy currents and hardness testing for evaluation of steel decarburizing. NDT & E International. 2006;39(8):652-660.

18. Blaow M, Evans J, Shaw B. Surface decarburisation of steel detected by magnetic Barkhausen emission. Journal of materials science. 2005;40(20):5517-5520.
19. Zhu W, Yin W, Dewey S, et al. Modeling and experimental study of a multi-frequency electromagnetic sensor system for rail decarburisation measurement. NDT & E International. 2017;86:1-6.
20. Kahrobaee S, Jahantigh Fard E. Characterization of Hadfield Steels Subjected to Various Heat-Treating Processes by Nondestructive Eddy Current Method. Russian Journal of Nondestructive Testing. 2020;56:151-160.
21. Kahrobaee S, Zohourvahid Karimi E. Characterisation of work-hardening in Hadfield steel using non-destructive eddy current method. Nondestructive Testing and Evaluation. 2019;34(2):178-192.
22. Shull PJ. Nondestructive evaluation: theory, techniques, and applications. CRC press; 2002.

Figure Captions

Fig. 1. Block diagram of the proposed measurement setup.

Fig. 2. Hardness profiles of the samples austenitised for 1, 2, 3 and 4 hours (the decarburised depths were obtained as 35, 55, 65 and 110 µm, respectively).

Fig. 3. Optical images of the steel surface during a) 0, b) 1, c) 2, d) 3 and e) 4 hours austenitising treatment in the air furnace (the cross sections of the samples were etched with Vilella's reagent (2 g picric acid and 5 mL HCl in 100 mL ethyl alcohol).

Fig. 4. a) SEM micrograph of a cross section of the Hadfield steel subjected to austenitisation time of 4 hours; b) austenitic phase of core and c-e) martensitic phase of decarburised layer.

Fig. 5. X-ray diffraction patterns of the as-received samples and the ones austenitised for different periods of time extracted from less than 20 micrometers below the surface.

Fig. 6. a) Induced MFL voltage vs. time for different austenitising time and b) MFL Vp-p vs. decarburisation depth.

Fig. 7. a) Magnetic flux density (B) vs. magnetic field strength (H) for different decarburisation depths and b) the maximum of B vs. decarburisation depth.

Fig. 8. The eddy current results, a) RMS voltage, b) normalised impedance and c) phase angle, all vs. decarburisation depth.

Fig. 9. The normalised parameters from the three MFL, BH and EC subsystems by the as-received sample with respect to the decarburisation depth.

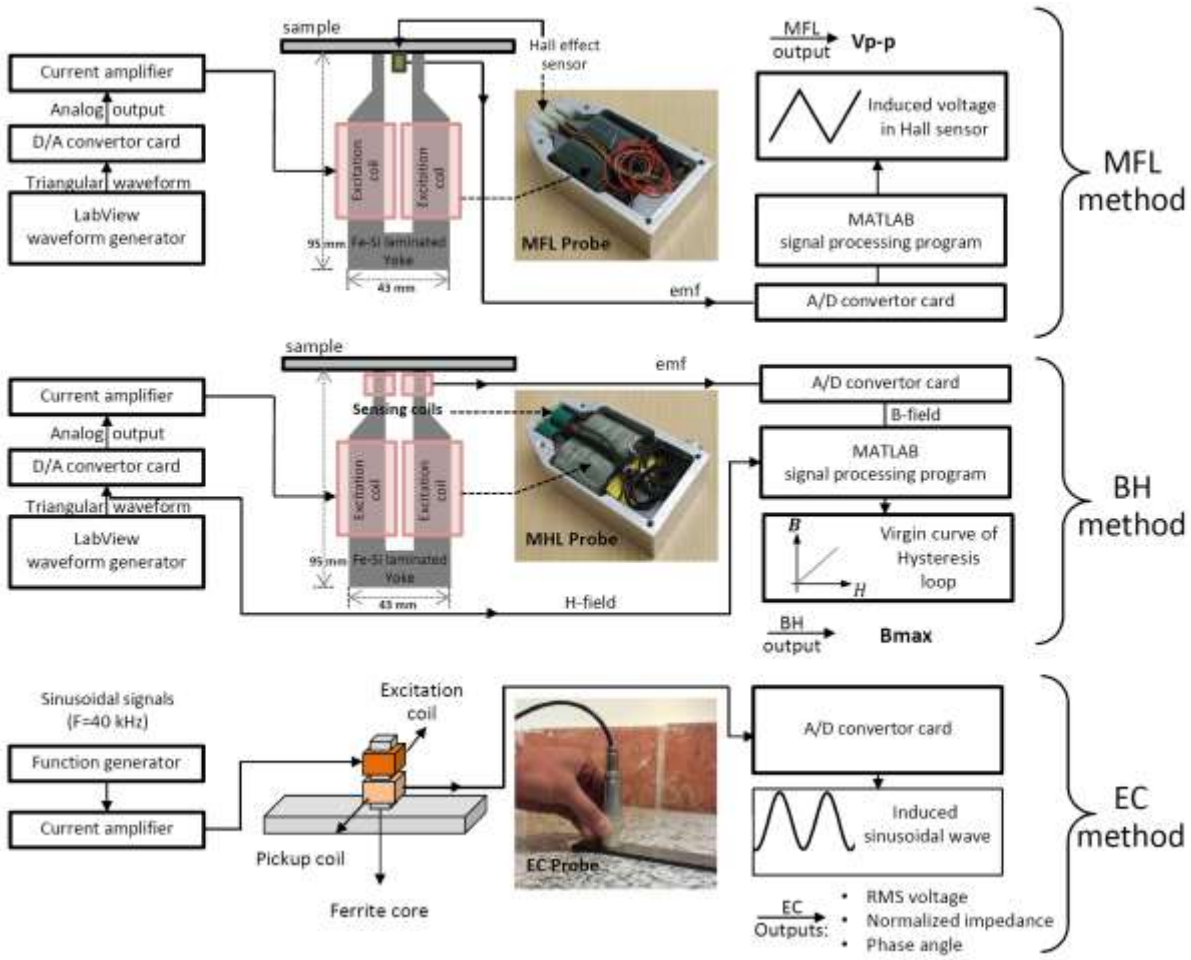
sample
Hall effect sensor
Current amplifier
Analog output
D/A convertor card
Triangular waveform
LabView waveform generator
Excitation coil
Excitation coil
95 mm
Fe-Si laminated Yoke
43 mm
MFL Probe
MFL output
Vp-p
Induced voltage in Hall sensor
MATLAB signal processing program
A/D convertor card
emf
MFL method
sample
emf
Current amplifier
Sensing coils
A/D convertor card
B-field
Analog output
D/A convertor card
MATLAB signal processing program
Triangular waveform
LabView waveform generator
Excitation coil
Excitation coil
MHL Probe
B
H
Virgin curve of Hysteresis loop
95 mm
Fe-Si laminated Yoke
43 mm
H-field
BH output
Bmax
BH method
Sinusoidal signals (F=40 kHz)
Excitation coil
Function generator
Current amplifier
Pickup coil
Ferrite core
EC Probe
A/D convertor card
Induced sinusoidal wave
EC Outputs:
RMS voltage
Normalized impedance
Phase angle
EC method

Fig.1

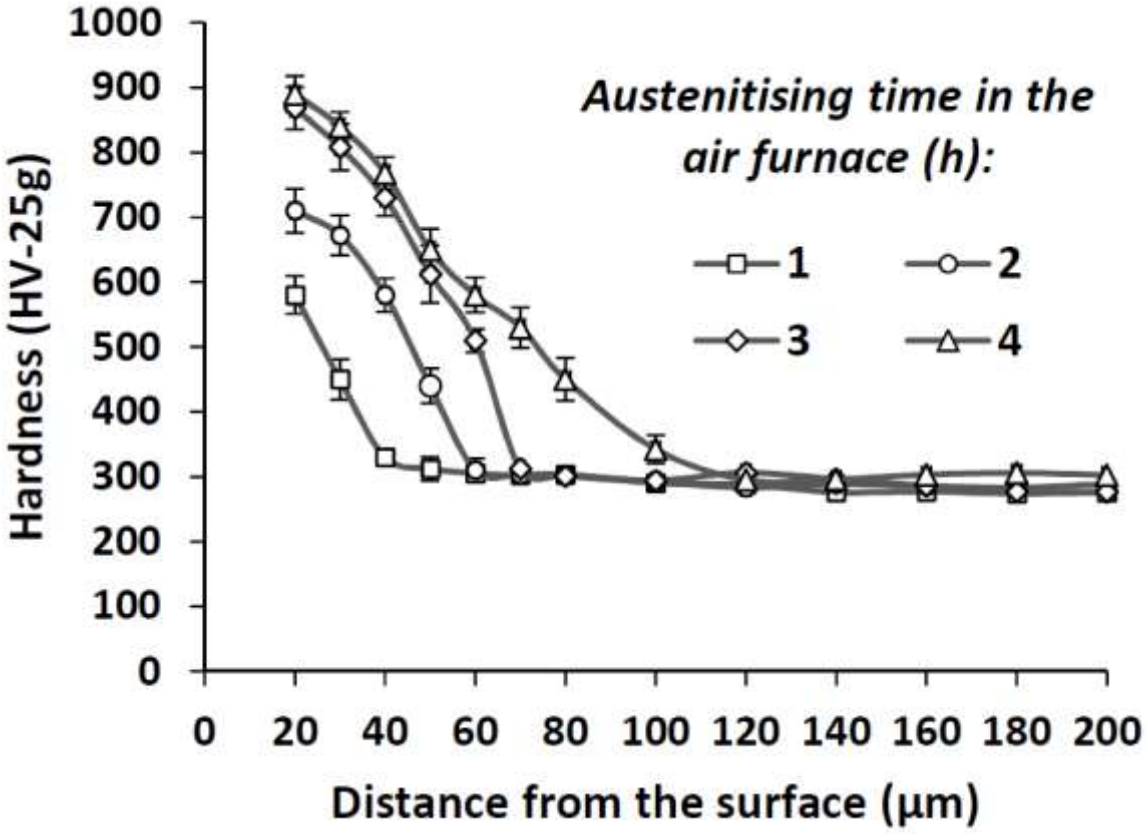
Hardness (HV-25g)
1000
900
800
700
600
500
400
300
200
100
0
0
20
40
60
80
100
120
140
160
180
200
Distance from the surface (µm)
Austenitising time in the air furnace (h):
1
2
3
4

Fig 2

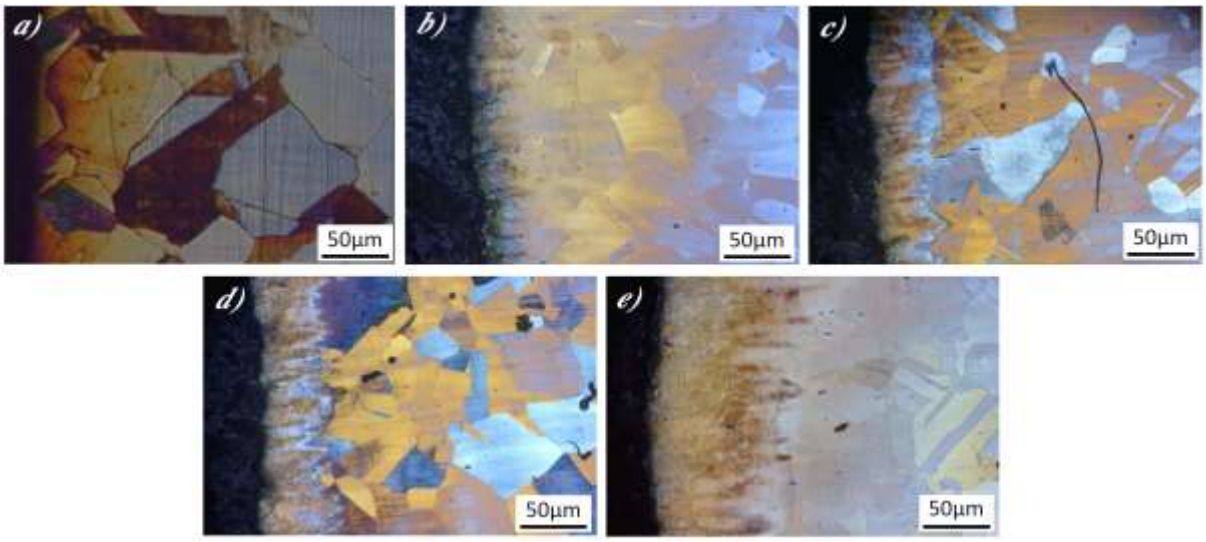

Fig 3.

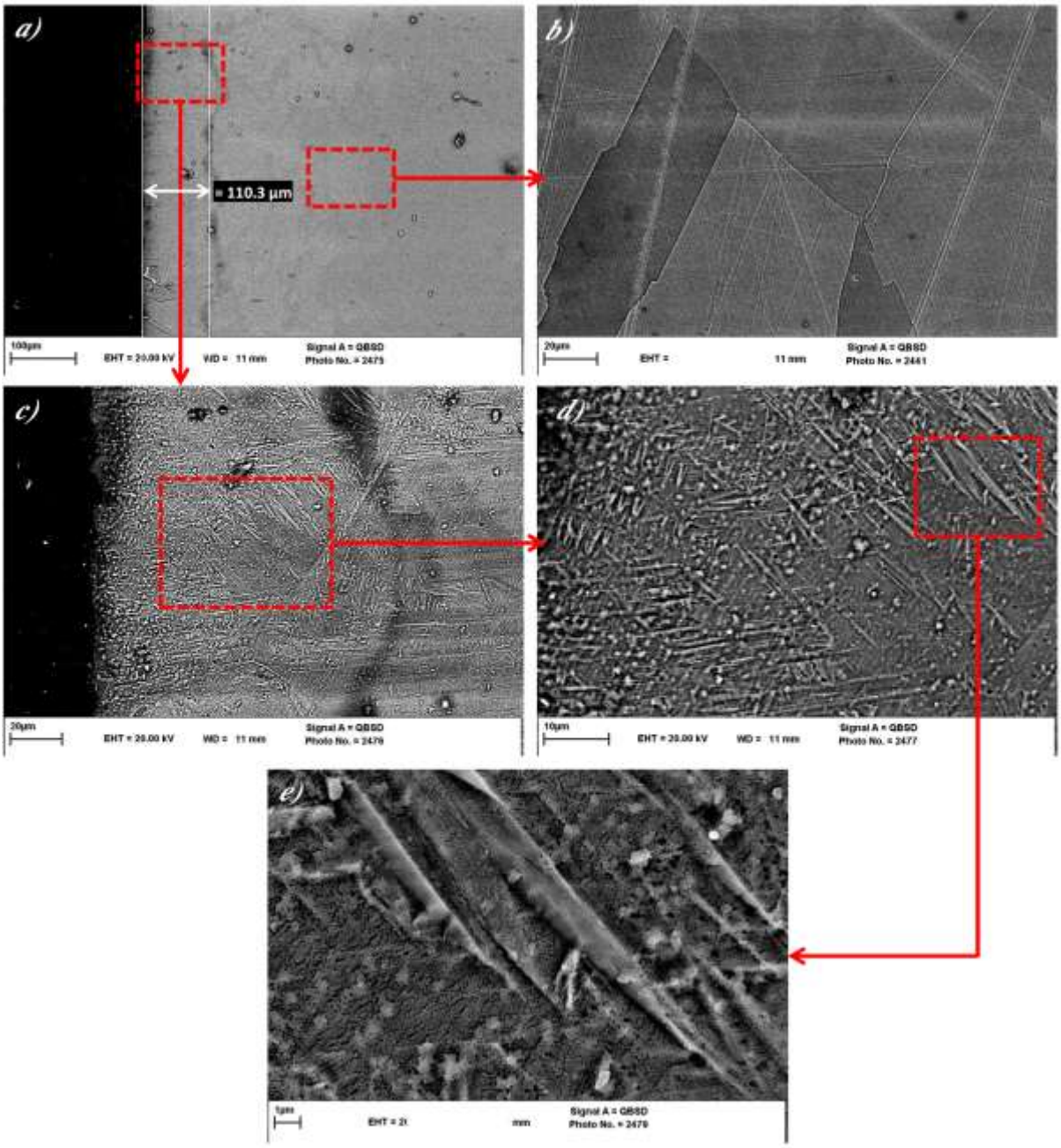

Fig. 4

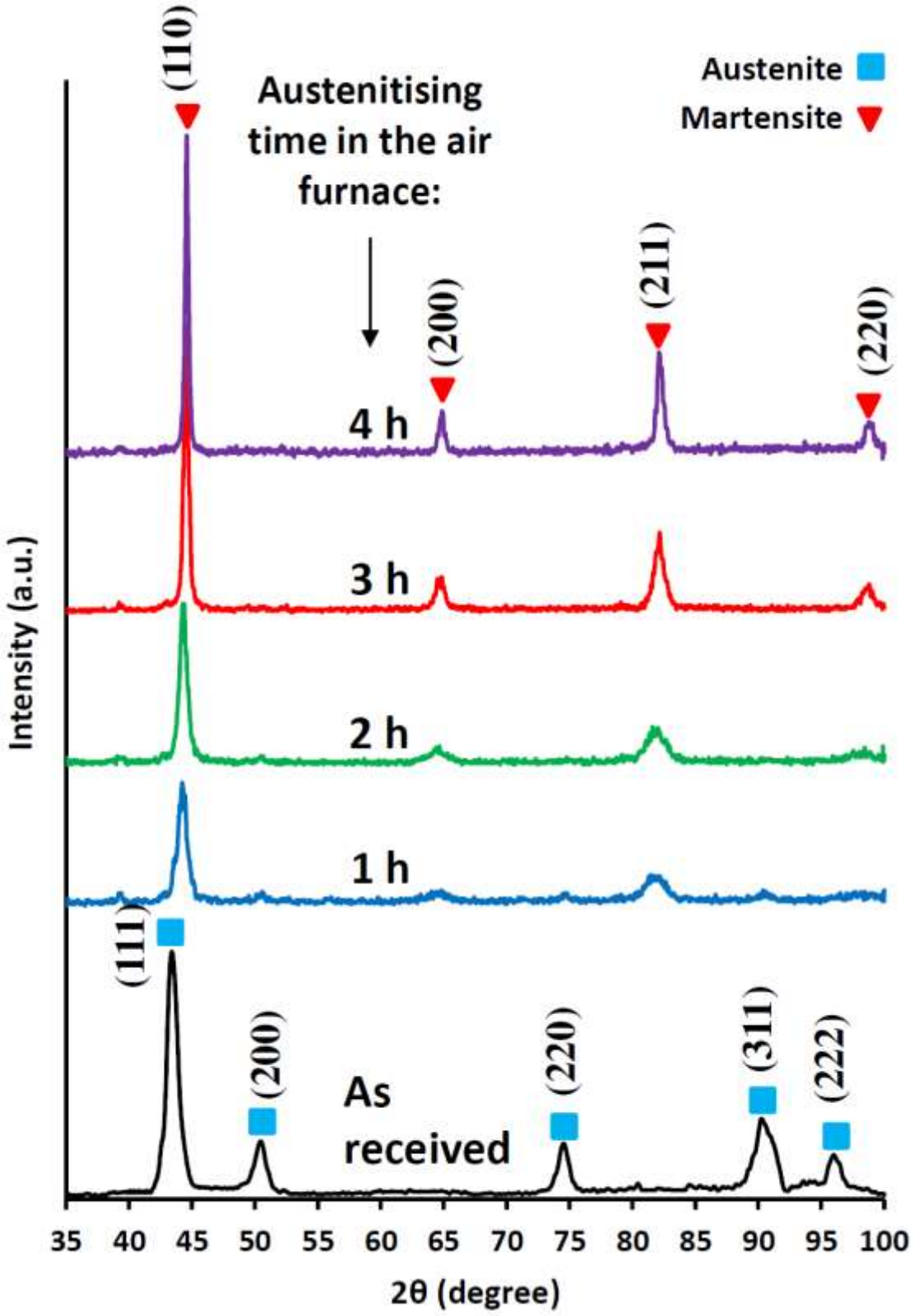
Austenite
Martensite
Austenitising time in the air furnace:
(110)
(200)
(211)
(220)
4 h
3 h
2 h
1 h
(111)
(200)
(220)
(311)
(222)
As received
Intensity (a.u.)
35 40 45 50 55 60 65 70 75 80 85 90 95 100
2θ (degree)

Fig 5.

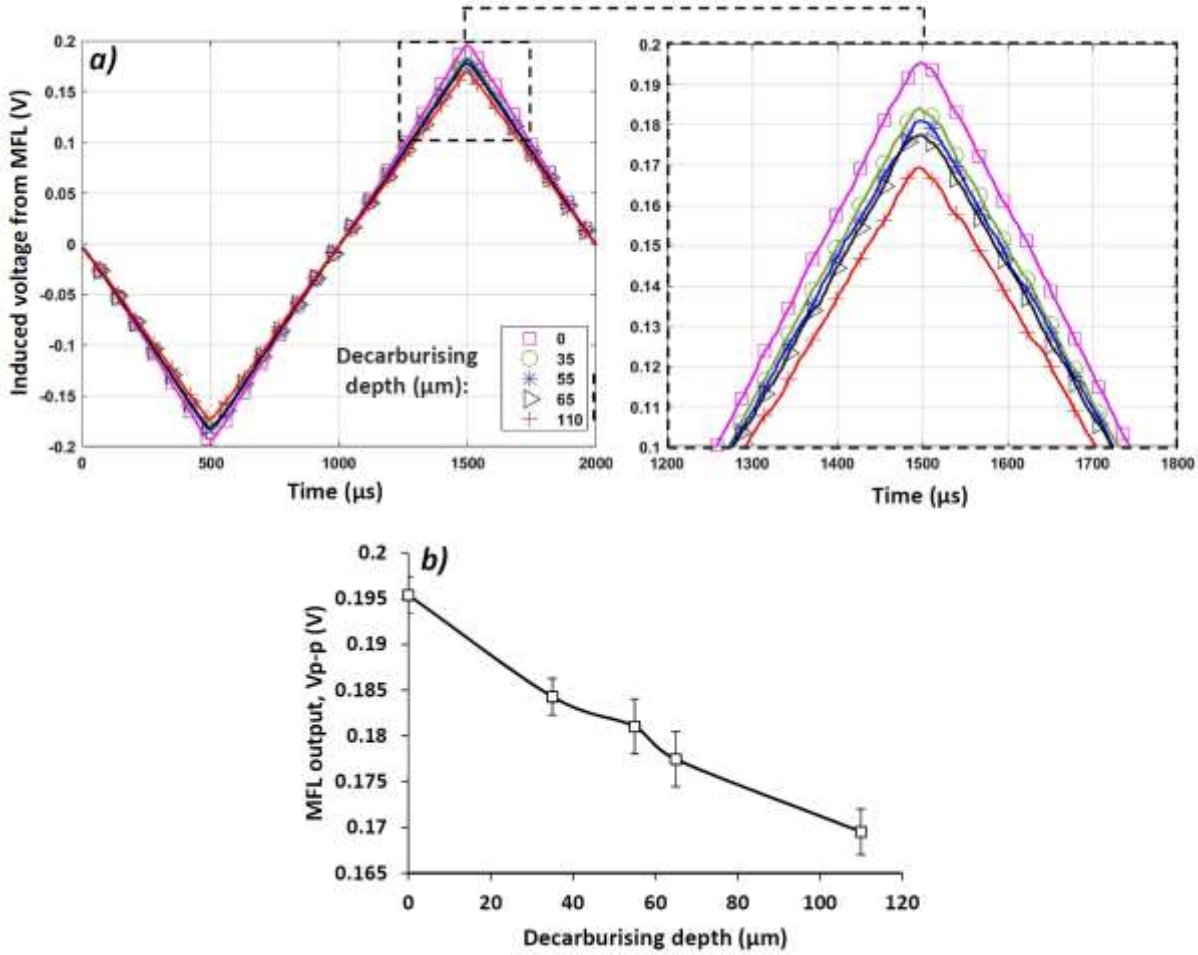
a)
Induced voltage from MFL (V)
Time (µs)
Decarburising depth (µm):
0
35
55
65
110
b)
MFL output, Vp-p (V)
Decarburising depth (µm)

Fig 6.

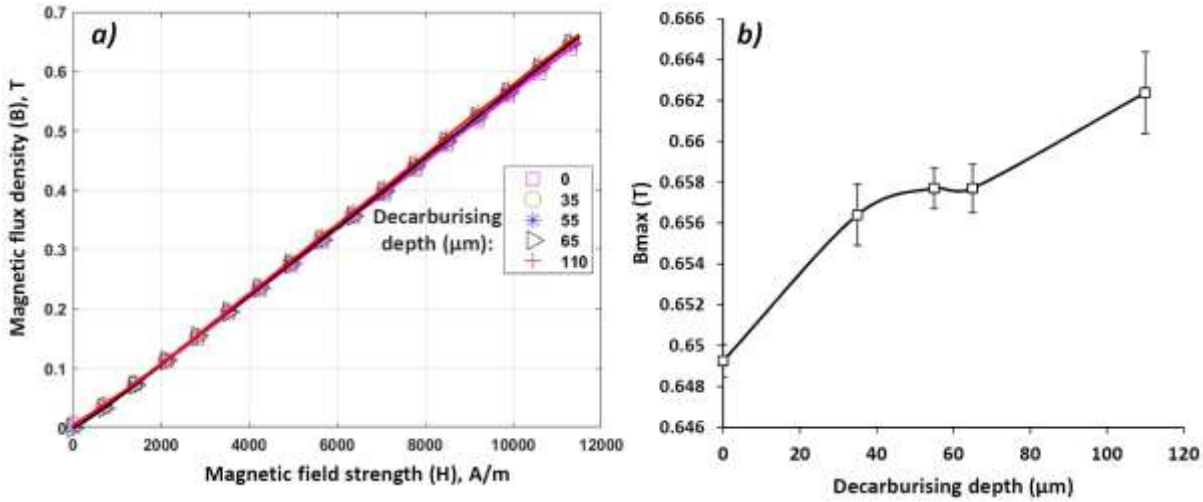
a)
Magnetic flux density (B), T
Magnetic field strength (H), A/m
Decarburising depth (µm):
0
35
55
65
110
b)
Bmax (T)
Decarburising depth (µm)

Fig 7.

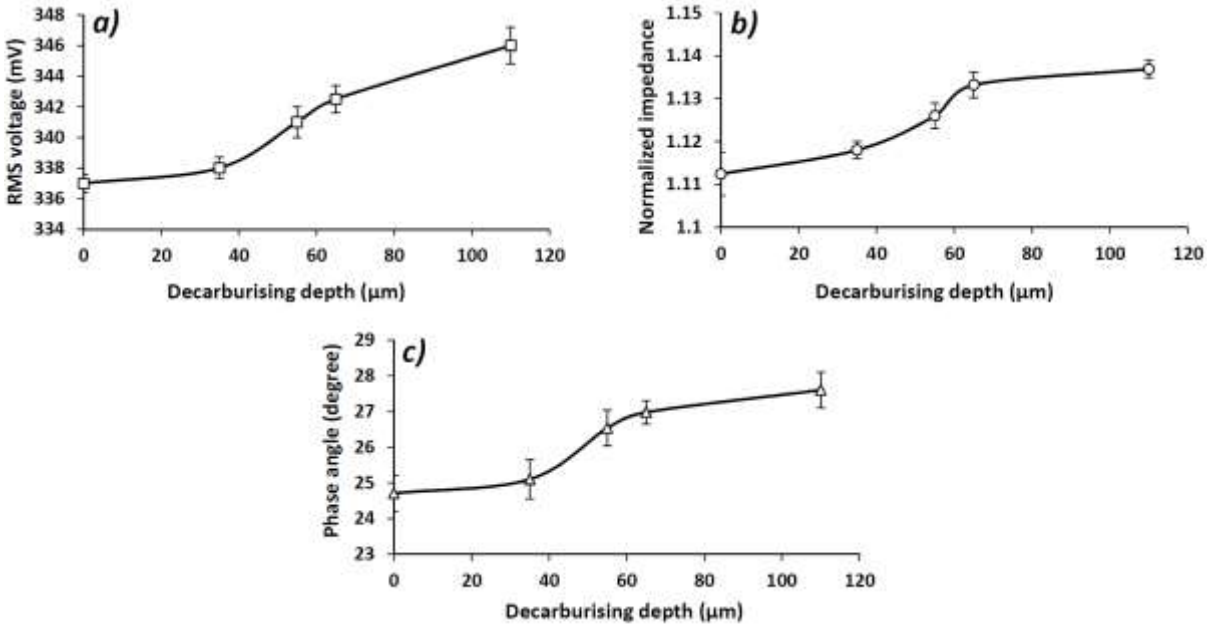
a)
RMS voltage (mV)
348
346
344
342
340
338
336
334
0
20
40
60
80
100
120
Decarburising depth (µm)
b)
Normalized impedance
1.15
1.14
1.13
1.12
1.11
1.1
0
20
40
60
80
100
120
Decarburising depth (µm)
c)
Phase angle (degree)
29
28
27
26
25
24
23
0
20
40
60
80
100
120
Decarburising depth (µm)

Fig 8.

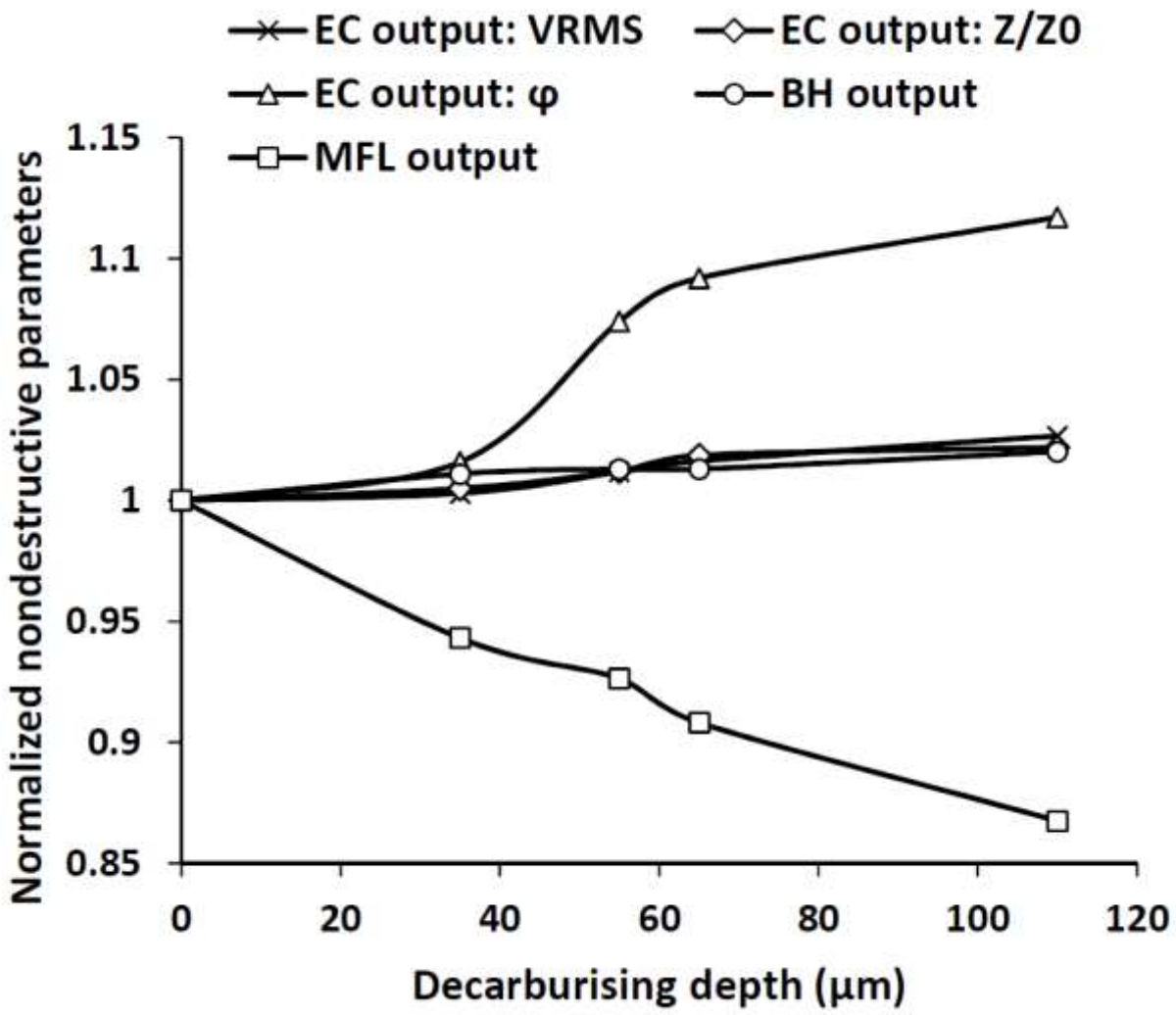
EC output: VRMS
EC output: Z/Z0
EC output: φ
BH output
MFL output
Normalized nondestructive parameters
1.15
1.1
1.05
1
0.95
0.9
0.85
0
20
40
60
80
100
120
Decarburising depth (µm)

Fig 9.

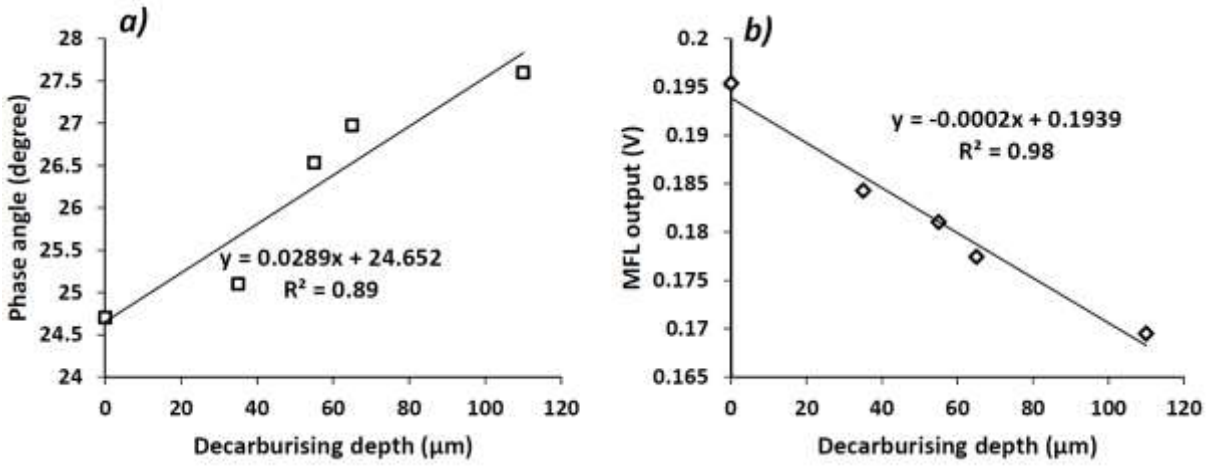
a)
Phase angle (degree)
28
27.5
27
26.5
26
25.5
25
24.5
24
y = 0.0289x + 24.652
R² = 0.89
0
20
40
60
80
100
120
Decarburising depth (µm)
b)
MFL output (V)
0.2
0.195
0.19
0.185
0.18
0.175
0.17
0.165
y = -0.0002x + 0.1939
R² = 0.98
0
20
40
60
80
100
120
Decarburising depth (µm)

Fig 10.